Journal of
Ceramic Science
and Technology

J. Ceram. Sci. Technol., **09** [1] 93-98 (2018)
DOI: 10.4416/JCST2017-00046
available online at: http://www.ceramic-science.com

Short Communication

Reinforcement Mechanisms in Yttria-Ceria-Co-Stabilized Zirconia-Alumina-Strontium Hexaaluminate Composite Ceramics

F. Kern*, A. Gommeringer

University of Stuttgart, Institute for Manufacturing Technologies of Ceramic Components and Composites, Allmandring 7B, D-70569 Stuttgart, Germany

received June 30, 2017; accepted September 12, 2017

Abstract

Composite ceramics with 1 mol% yttria and 6 mol% ceria co-stabilized zirconia matrix were reinforced with 10 vol% alumina and 10 vol% *in situ*-formed strontium hexaaluminate. Samples were shaped by means of slip casting in plaster molds and sintered in air for 3 – 72 h at 1500 °C. Full density and highest fracture resistance were achieved in overfired material while the maximum strength of 900 MPa was obtained at a dwell of 12 h. The high fracture resistance up to 10.4 MPa√m results from contributions of different reinforcement mechanisms: microcracking, crack bridging, crack deflection and – predominantly – transformation toughening.

Keywords: Zirconia, platelets, microstructure, mechanical properties

I. Introduction

Since Garvie [1] reported on the first high-strength zirconia ceramics in 1975, two main types of partially stabilized zirconia ceramics which exploit the effect of transformation toughening have been developed. In the PSZ (partially stabilized zirconia) types such as Mg-PSZ and Ca-PSZ small tetragonal precipitates in a coarse-grain cubic matrix provide the toughening [2]. In the TZP (tetragonal zirconia polycrystals)-type materials such as Y-TZP and Ce-TZP, the microstructure is fine-grained and consists predominantly of tetragonal phase. Y-TZP and Ce-TZP show completely adverse mechanical properties and low-temperature degradation (LTD) characteristics [3]. Y-TZP has high strength, moderate toughness and a low LTD resistance, while Ce-TZP is extremely tough, has moderate strength and is LTD-resistant. In order to combine the favorable properties of both materials, co-stabilization can be applied [4,5]. Lin carried out very systematic studies leading to hardness-, toughness- and strength maps of Y-Ce-TZP materials depending on stabilizer contents [6,7]. In these maps, the strength maxima of ~1000 MPa were found at compositions around 2Y-4Ce-TZP, the toughness maximum of 20 MPa√m was identified at 0.8Y-5.5Ce-TZP. The corresponding strength and toughness values of these two materials are, however, inferior. A material composition offering a good compromise between strength and toughness should be positioned in the transition range between flaw-size and transformation-dominated failure [8]. It was shown that a composition of 1.25Y6Ce-TZP can achieve a strength/toughness combination of 1000 MPa and 9 MPa√m [9]. Another concept to improve the strength of TZP materials is the addition of alumina, which leads to ATZ (alumina toughened zirconia). Y-TZP/alumina composites may reach strength of > 2 GPa at unchanged moderate toughness [10]. In Ce-TZP, addition of alumina boosts the strength but reduces the toughness considerably. Cutler therefore introduced *in situ* reinforcement with strontium hexaaluminate (SA6) platelets to retain the toughness but improve the strength [11]. It was shown that high fractions of 30 vol% SA6 provide toughness, but weak interfaces between SA6 and zirconia lead to a CMC-like fracture behavior with limited strength [12]. In recent studies on more sophisticated 12Ce-TZP/alumina and 12Ce-TZP/alumina/SA6 composites carried out by Touaiher [13], toughness of 10 MPa√m was achieved, the measured strength varied, however, strongly (600 – 1600 MPa) depending on loading conditions. This study is the first one published to combine Y-Ce-costabilization with the concept of *in situ* platelet reinforcement in order to obtain a first impression of the contributions of the prevalent reinforcement mechanisms.

II. Experimental

The starting powders for the study were unstabilized zirconia (S_{BET} = 7 m²/g, d_{50} = 350 nm), α-alumina (S_{BET} = 8 m²/g, d_{50} = 300 nm), ammonium cerium (IV) nitrate (purity 99 %), strontium carbonate (purity 99 %) and yttria (purity 99.9 %). Yttria and strontia were separately dissolved in 5N HNO_3. Monoclinic zirconia was coated via the nitrate route according to a modified procedure [14] first described by Yuan [15]. A batch of 500 g stabilizer-coated zirconia was produced, which after calcination at 600 °C contained 1 mol% Y_2O_3 and 1.5 mol% SrO. Nanoscale ceria was prepared by decomposition of ammonium ceri-

* Corresponding author: frank.kern@ifkb.uni-stuttgart.de

um (IV) nitrate at 600 °C in air. The aqueous dispersion for the slip casting was produced by milling a batch of 500 g powder mixture containing commensurate amounts of Y-Sr-TZP, ceria and alumina to obtain a composite containing 1Y-6Ce-TZP with two dispersions of 10 vol% alumina and 10 vol% SA6 after sintering (1Y-6Ce-10A-10SA6). 300 ml water was used as dispersion medium with an addition of 1 m% (in respect of powder) commercially available surfactant and 1 m% binder, the mixture was attrition-milled for 4 h with Y-TZP milling balls (d = 2 mm), then milling media were separated and the dispersion was de-gassed at 200 mbar for 2 h. Samples were cast on a plaster plate using silicone molds of 45 × 35 mm² in width. After drying, the plates obtained were debinded in air at 800 °C for 3 h and sintered in air at 1500 °C for 3 – 72 h (Thermconcept, Germany). The plates were subsequently lapped and cut into bending bars measuring 4 mm × 2 mm width and ~ 25 mm length (Struers Accutom, Denmark). Bending bars were lapped with 15-µm diamond suspension and polished with 3-µm diamond suspension to a mirrorlike finish on the tensile side (Struers Rotopol, Denmark). Edges were beveled with a 20-µm diamond disk. The test protocol included measurement of density with the buoyancy method (2 entire plates before cutting), determination of Young's modulus E by means of sonic excitation (2 entire plates before cutting, IMCE, Belgium) and the measurement of Vickers hardness HV10 (5 indents, Bareiss, Germany). Four-point bending strength σ_{4pt} was measured in a 20/10 mm setup (10 bars, Zwick, Germany, crosshead speed 0.5 mm/min). The fracture resistance K_{IC} was determined by means of indentation strength in bending (ISB), samples were notched with a HV10 indent in the middle of the polished tensile side and the residual strength was measured in the same 4pt setup (cracks parallel and perpendicular to the sides, 5 samples, crosshead speed 2.5 mm/min). Toughness was calculated from residual strength using the model of Chantikul [16]. Resistance to subcritical crack growth K_{I0} was determined by means of stable indentation crack growth in bending (SIGB) according to Braun [17] and Dransmann [18] (2 samples each, 4 indents/bar, cracks parallel and perpendicular to the sides, storage 1 week prior to testing, crosshead speed 5 mm/min). The microstructure was studied with SEM (Zeiss Gemini, Germany, secondary electrons, 10 kV) on thermally etched samples (500 K/min to 1350 K/10 min in air). The phase composition was determined by means of XRD by integrating the monoclinic (-111) and (111) and the tetragonal (101) peaks in the 27 – 33° 2θ range ((Bruker AXS D8, Germany, Bragg-Brentano theta-2theta, CuKα_1), quantitative analysis was carried out using the calibration curve of Toraya [19]. The size of the transformation zone h was calculated according to Kosmac [20]. The transformation toughness increment K_{IC}^T was determined according to McMeeking [21] with a transformation efficiency constant X = 0.27, which is typical for Y-TZP and relates to predominantly dilatoric transformation [22].

III. Results and Discussion

The relative density of the TZP composites increases from 95 % at 3 h to 100 % at 72 h dwell and consequently the Young's modulus E and the Vickers hardness HV10 also rise (Fig. 1). The value of Young's modulus at full density is somewhat lower than the expected value according to the rule of mixture (230 GPa). The hardness of the composites is lower than the hardness of alumina-doped Y-TZP (1300 HV10)[2]. The strength σ_{4pt}, fracture toughness K_{IC} and the resistance to subcritical crack growth (threshold toughness) K_{I0} values are plotted in Fig. 2. The bending strength rises from 810 MPa at 3 h dwell to its peak level of 900 MPa at 12 h dwell and then declines slightly in the oversintered (72 h) material. The fracture toughness K_{IC} rises with increasing dwell from 7.7 MPa√m at 3 h to 10.4 MPa√m at 72 h. Compared to standard 3Y-TZP (K_{IC} = 5 – 6 MPa√m) employed in dental restorations [23], this is a very attractive toughness range. The measurement of threshold toughness K_{I0} with the SIGB technique reveals an interesting detail. K_{I0} stays constant at a level of 4.5 ± 0.15 MPa√m over the whole dwell range investigated. This means that the increase of toughness observed with increasing dwell is caused by rising contributions of process zone mechanisms such as transformation toughening, crack bridging and deflection and microcracking. Another important item of information coming from the strength and toughness data is the fatigue limit, i.e. the stress the material can bear under repeated loading conditions or under constant load. The fatigue limit [24] $\sigma_{FL} = \sigma_{4pt} \cdot K_{I0}/K_{IC}$ is almost constant between 3 h and 12 h dwell, reaches a flat maximum of 466 MPa at 12 h dwell and drops to 388 MPa at 72 h.

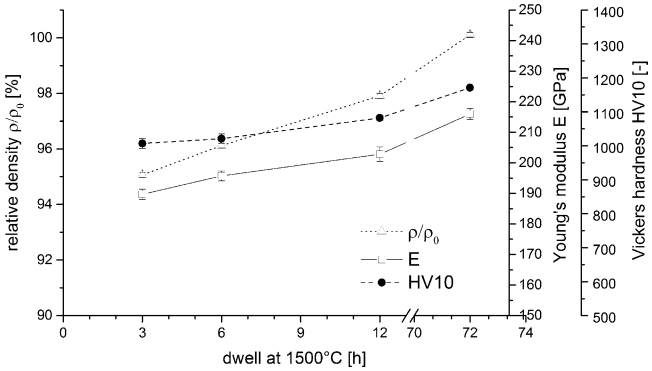

Fig. 1: Relative density ϱ/ϱ0, Young's modulus E and Vickers hardness HV10 of 1Y6Ce-10A-10SA6 vs. dwell at 1500 °C sintering temperature.

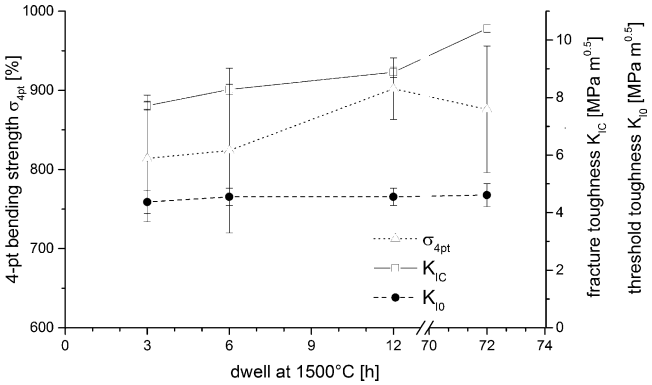

Fig. 2: 4pt bending strength σ_{4pt}, fracture toughness K_{IC} and threshold toughness K_{I0} of 1Y6Ce-10A-10SA6 vs. dwell at 1500 °C sintering temperature.

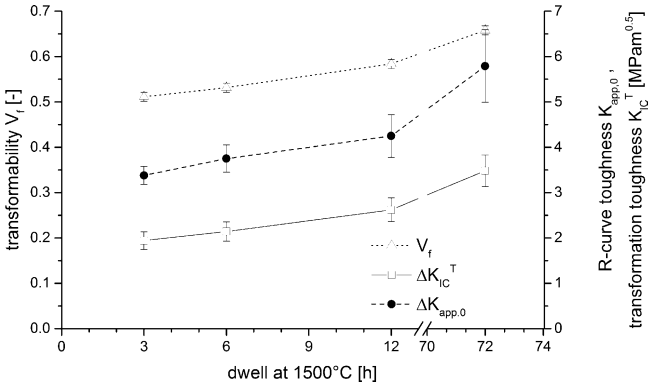

Fig. 3: Transformability V_f, transformation toughness increment ΔK_{IC}^T and R-curve-dependent toughness increment $K_{app,0}$ of 1Y6Ce-10A-10SA6 vs. dwell at 1500 °C sintering temperature.

The transformability of zirconia V_f, the transformation toughness increment K_{IC}^T and the toughness caused by R-curve effects $K_{app,0}$ (SIGB-test) are shown in Fig. 3. The information on phase composition allows calculation of the transformation zone height [20] h and the transformation toughness increment[21] $K_{IC}^T = 0.8 \cdot E \cdot V_f \cdot \sqrt{h} \cdot \varepsilon_T \cdot X/(1-\nu)$ (E, V_f, h are measured values, the transformation strain [22] $\varepsilon_T = 0.05$, the transformation efficiency X is 0.27 [22]). All samples were entirely tetragonal in as-fired state. The measured monoclinic content in the fracture phase thus represents the transformability V_f. V_f rises progressively with increasing dwell from 51 % at 3 h to 66 % at 72 h dwell. Consequently, the calculated transformation toughness increment K_{IC}^T also rises in the same dwell range from 2 to 3.5 MPa$\sqrt{m}$. The comparison of K_{IC}^T with the R-curve-dependent part of toughness $K_{app,0}$ determined in the SIGB experiment can be exploited to estimate the toughness contributions by other mechanisms. Calculation of crack bridging and crack deflection contributions require detailed information on microstructure. As the CTE of the alumina and SA6 dispersions is lower than for CTE, we can assume that the residual-stress-induced toughness is negative. According to Taya [25], we may estimate the toughness reduction as $\Delta K_{RS} = -0.2 - 0.3$ MPa$\sqrt{m}$. Crack bridging by SA6 platelets and alumina provides extra-toughness. According to Becher [26], the crack bridging can be estimated as $\Delta K_{CB} = +1$ MPa$\sqrt{m}$ so that both effects in total amount to +0.7 – 0.8 MPa$\sqrt{m}$ which, considering the standard deviations, only explains a part of the increment $K_{app,0} - \Delta K_{IC}^T$. Fig. 4 shows the microstructure of material sintered at 12 h (A) and 72 h (B) together with images of cracks (C, D) introduced by Vickers indents (crack progression from lower left to upper right corner). The SA6 platelets are typically rod-shaped with an average length between 3 – 5 µm and a width 0.6 – 1 µm. Platelet dimensions do not change with dwell. In the case of the materials sintered for 3 – 6 h there are small globular zirconia inclusions of 200 nm in diameter trapped within the platelets. At longer dwell, these inclusions are increasingly eliminated. At 72 h no more inclusions can be observed. As can be expected, the TZP matrix progressively coarsens with increasing sintering time. Grain growth is, however, relatively moderate between 3 h (1.9 ± 0.1 µm) and 12 h (2.2 ± 0.2 µm). At 72 h dwell, the average grain size increases to 3.5 ± 0.3 µm. The alumina dispersion also shows some coarsening. At 3 h dwell, most grains still have the grain size of the starting powder (0.3 – 0.5 µm), while at 72 h the number of alumina grains is significantly reduced while their diameter has increased to 1 – 1.5 µm. All dispersions have a lower coefficient of thermal expansion CTE than the matrix. Coarsening effects do not affect the level of average hydrostatic stress but the local stress in the vicinity of the particles/platelets which increases by a ratio R^3/r^3 with R the radius of the particle and r the distance from the center of the particle [27]. In the case of the SA6 platelets, stress fields around the particles are anisotropic not only because of their high aspect ratio but also because of their crystallographic anisotropy. Papst [28] has shown that for alumina the CTE along the a-axis (8.2×10^{-6} K^{-1}) is ~ 10 % lower than along the c-axis (9×10^{-6} K^{-1}). There are no literature data available for SA6 but assuming *a priori* the same dependence for SA6, this enhances the tensile stresses in the matrix along the growth direction of the platelets. The stress concentration is thus highest at the tips of the platelet, this is the location where microcracks are induced by cooling stress (Fig. 4B). This trend to form microcracks is enhanced with increasing grain size of the matrix as grains are more stable than grain boundaries and fewer grain boundaries are available that could distribute the stress. Consequently, the concentration of pre-existing microcracks and their size grows with increasing dwell. Besides the microcracks along the TZP/TZP grain boundaries, circumferential microcracks or at least weakened grain boundaries can be observed around alumina particles. Evidently in SEM images alumina particles intersected during polishing are uplifted during thermal etching. The existence of microcracks also helps to explain the lower than expected Young's modulus of the materials. Fig. 4C and 4D show the typical reinforcement effects. Crack deflection at SA6 inclusions is not very frequently observed while large alumina grains always lead to crack deflection and de-bonding at the interface. As both alumina (E ~ 385 GPa) and SA6[29] (290 GPa) have a higher Young's modulus than the matrix, crack deflection is favored [30]. It seems, however, that the TZP/SA6 grain boundaries are relatively strong. This together with the moderate cohesive strength of the hexaaluminate [31] leads to fracture of the platelets if they are hit by the crack perpendicularly. In Fig. 4C the crack hits a platelet in 90° direction and enters the platelet. Owing to the layered structure of the aluminate, the crack path through the platelet is not straight but graded. After exiting the platelet, the crack runs along the SA6/TZP interface for 0.5 µm and then proceeds along a (weakened) TZP/TZP grain boundary in an angle of < 90°. Then the crack enters another smaller SA6 platelet and proceeds lengthwise through the platelet rather than proceeding along the SA6/TZP grain boundary. At the same time, the back side of the platelet delaminates from the TZP and a small secondary crack running transgranularly into the TZP is stopped after a few 100 nm owing to the high toughness of the matrix. Fig. 4D shows multiple crack branching among other effects. This redistribution of the energy of the primary crack into the surrounding volume – which is weakened locally by microcracks – is

observed very frequently and provides additional toughness especially in the materials sintered for 12 h and more. With the information from microstructure the calculation of toughness increments can be completed. After adding $\Delta K_{IC}{}^{T} + \Delta K_{CD} + \Delta K_{CB}$ to the balance. there is still an unexplained toughness increment of 0.7 – 0.9 MPa√m at 3 – 12 h dwell and 1.6 MPa√m at 72 h dwell. Taking into account the information on microstructure and the observed interaction of the cracks with the elements of the microstructure, it may be assumed that this yet unexplained increment ΔK_{MC} is caused by microcracks. Microcracking typically is a very powerful toughening mechanism [32]. The relatively moderate toughness contribution here is probably caused by the fact that the primary reinforcement by transformation toughening is associated with volume expansion of the zone around the crack, which actually should close the microcracks to a certain extent, so that toughening and microcracking are not fully additive here. Existence of a microcrack network also seems to be responsible for the limited strength of the materials as microcracks not only enhance toughness but also constitute structural defects.

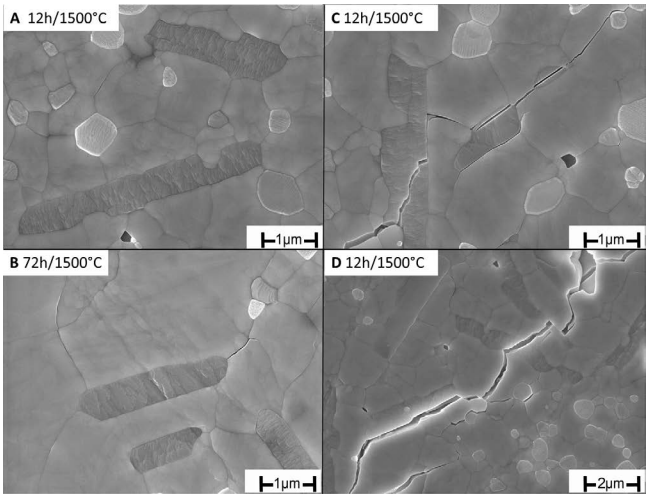

Fig. 4: SEM images showing microstructure and crack propagation in 1Y6Ce-10A-10SA6.

IV. Conclusions

The composite material observed is a good model material to study the contribution and interaction of different toughening mechanisms in ceramics. As shown, the high toughness observed in 1Y6Ce-10A-10SA6 composites is based on four process zone mechanisms in the following order: transformation toughening > crack bridging ≅ microcracking > crack deflection by residual stress (negative). While crack bridging and crack deflection show only negligible changes with the evolution of microstructure (coarsening), the transformation toughening and microcracking are enhanced at increasing matrix grain size. The total toughness can be satisfactorily explained based on an additive model as proposed by Evans [32] and does not require considering synergistic effects [33]. Microcracks do, however, provide less toughness than expected. For the practical application in e.g. dental implants it may be stated that the chosen formulation is, however, too tough and that extensive R-curve effects provide high reliability in case of catastrophic failure but no significant improvement compared to conventional 3Y-TZP with regard to fatigue.

Acknowledgements

The authors would like to thank G. Maier (XRD) and F. Predel (SEM) of Max Planck Institute Stuttgart for their assistance. This research did not receive any specific grant from funding agencies in the public, commercial, or not-for-profit sectors.

References

1 Garvie, R.C., Hannink, R.H., Pascoe, R.T.: Ceramic steel, *Nature,* **258,** 703 – 704, (1975).

2 Hannink, R.H.J., Kelly, P.M., Muddle, B.C.: Transformation toughening in zirconia-containing ceramics, *J. Am. Ceram. Soc.*, **83**, [3], 461 – 87, (2000).

3 Chevalier, J., Drouin, J.M., Cales, B.: Low-temperature aging of Y-TZP ceramics, *J. Am. Ceram. Soc.*, **82**, [8], 2150 – 54, (1999).

4 Vleugels, J., Xu, T., Huang, S., Kan, Y., Wang, P., Li, L., Van der Biest, O.: Characterization of (Nd,Y)-TZP ceramics prepared by a colloidal suspension coating technique, *J. Eur. Ceram. Soc.,* **27**, 1339 – 1343, (2007).

5 Kern, F: Ytterbia-neodymia-costabilized TZP—Breaking the limits of strength-toughness correlations for zirconia? *J. Eur. Ceram. Soc.*, **33**, 965 – 73, (2013).

6 Lin, J.-D., Duh J.-G.: Correlation of mechanical properties and composition in tetragonal CeO_2-Y_2O_3-ZrO_2 ceramic system, *Mat. Chem. Phys.,* **78**, 246 – 252, (2003).

7 Lin, J.-D., Duh J.-G.: Fracture toughness and hardness of ceria- and yttria-doped tetragonal zirconia ceramics, *Mat. Chem. Phys.*, **78**, 253 – 261, (2003).

8 Swain, M.V., Rose, L.R.F.: Strength limitations of transformation-toughened zirconia alloys, *J. Am. Ceram. Soc.*, **69**, [7], 511 – 18, (1986).

9 Kern, F., Gadow, R.: Thermoplastic forming of ceramic electrode substrates for deep brain stimulation, 24. Stuttgarter Kunststoffkolloquium Proceedings, IKT, University of Stuttgart, Stuttgart 2015.

10 Tsukuma, K., Ueda, K., Shimada, K.: Strength and fracture toughness of isostatically hot-pressed composites of Al_2O_3 and Y_2O_3-partially-stabilized ZrO_2, *J. Am. Ceram. Soc.*, **68**, [1], C4 – C5, (1985).

11 Cutler, R.A., Mayhew, R.J., Prettiman K.M., Virkar, A.: High-toughness Ce-TZP/Al_2O_3 ceramics with improved hardness and strength, *J. Am. Ceram. Soc.*, **74**, [1], 179 – 186, (1991).

12 Kern, F: A comparison of microstructure and mechanical properties of 12Ce-TZP reinforced with alumina and in situ formed strontium- or lanthanum hexaaluminate precipitates, *J. Eur. Ceram. Soc.*, **34**, [2], 413 – 23, (2013).

13 Touaiher, I., Saadaoui, M., Chevalier, J., Reveron, H.: Effect of loading configuration on strength values in a highly transformable zirconia-based composite, *Dental Materials*, **32**, 211 – 219, (2016).

14 Kern, F., Gadow, R.: Tough to brittle transition with increasing grain size in 3Yb-TZP ceramics manufactured from stabilizer coated nanopowders, *J. Jap. Ceram. Soc.*, **124**, 1083 – 1089, (2016).

15 Yuan, Z.X., Vleugels, J., Van der Biest, O.: Preparation of Y_2O_3-coated ZrO_2 powder by suspension drying, *J. Mat. Sci. Lett.*, **19**, 359 – 61, (2000).

16 Chantikul, P., Anstis, G.R., Lawn, B.R., Marshall, D.B.: A critical evaluation of indentation techniques for measuring fracture toughness: II, Strength method, *J. Am. Ceram. Soc.,* **64**, (9), 539 – 543, (1981).

[17] Braun, L.M., Bennison, S.J., Lawn, B.R: Objective evaluation of short-crack toughness curves using indentation flaws: Case study on alumina-based ceramics, *J. Am. Ceram. Soc.,* **75**, [11], 3049 – 57, (1992).

[18] Dransmann, G.W., Steinbrech, R.W., Pajares, A., Guiberteau, F., Dominguez-Rodriguez, A., Heuer, A.: Indentation studies on Y_2O_3-stabilized ZrO_2: II, toughness determination from stable growth of indentation-induced cracks, *J. Am. Ceram. Soc.*, **77**, [5], 1194 – 1201, (1994).

[19] Toraya, H., Yoshimura, M., Somiya, S.: Calibration curve for quantitative analysis of the monoclinic-tetragonal ZrO_2 system by X-ray diffraction, *J. Am. Ceram. Soc.*, **67**, [6], C119 – 21, (1984).

[20] Kosmac, T., Wagner, R., Claussen, N.: X-ray determination of transformation depths in ceramics containing tetragonal ZrO_2, *J. Am. Ceram. Soc.*, **64**, [4], C72 – 3, (1981).

[21] McMeeking, R.M., Evans, A.G.: Mechanics of transformation-toughening in brittle materials, *J. Am. Ceram. Soc.*, **65**, [5], 242 – 46, (1982).

[22] Kelly, P.M., Rose, L.R.F.: The martensitic transformation of ceramics – its role in transformation toughening, *Progr. Mat. Sci.*, **67**, 463 – 557, (2002).

[23] Kelly, J., Denry, I.D.: Stabilized zirconia as a structural ceramic: an overview, *Dental Materials,* **24**, 289 – 298, (2008).

[24] De Aza, A.H., Chevalier, J., Fantozzi, G., Schehl, M., Torrecillas, R.: Slow-crack-growth behavior of zirconia-toughened alumina ceramics processed by different methods, *J. Am. Ceram. Soc.,* **86**, 115 – 120, (2003).

[25] Taya, M., Hayashi, S., Kobayashi, A.S., Yoon, H.S.: Toughening of a particulate-reinforced ceramic-matrix composite by thermal residual stress, *J. Am. Ceram. Soc.*, **73**, [5], 1382 – 1391, (1990).

[26] Becher, P.F., Hsueh, C-H., Angelini, P., Tiegs, T.N.: Toughening behavior in whisker-reinforced ceramic matrix composites, *J. Am. Ceram. Soc.*, **71**, [12], 1050 – 61, (1988).

[27] Kingery, D., Bowen, H.K., Uhlmann, D.R.: Introduction to ceramics, 2nd ed., Wiley, New York, 1976.

[28] Papst, W., Gregorova, E.: Effective thermal and thermoelastic properties of alumina, zirconia and alumina-zirconia composite ceramics, in: New developments in materials science research, Nova Science Publishers Inc., New York, USA, 2007.

[29] Schmid, C., Lucchini, E., Sbaizero, O., Maschio, S.: The synthesis of calcium or strontium hexaluminate added ZTA composite ceramics, *J. Eur. Ceram. Soc.*, **19**, 1741 – 1746, (1999).

[30] He, M.H., Evens, A.G., Hutchinson, J.W.: Crack deflection at an interface between dissimilar elastic materials – the role of residual stresses, *Int. J. Solids Struct.*,**31**, [24], 3443 – 55, (1994).

[31] Chen, P.L., Chen, I.W.: In-situ alumina/aluminate platelet composites, *J. Am. Ceram. Soc.*, **75**, [9], 2610 – 2612, (1992).

[32] Evans, A.G.: Perspective on the development of high-toughness ceramics, *J. Am. Ceram. Soc.*, **73**, [2], 187 – 205, (1990).

[33] Amazigo, J.C., Budiansky, B.: Interaction of particulate and transformation toughening, *J. Mech. Phys. Solids*, **36**, 581 – 595, (1988).